A Reinvestigation of the Secondary Structure of Functionally Active vSGLT, the *Vibrio* Sodium/Galactose Cotransporter†

Eric Turk,*,‡ Oktay K. Gasymov,§ Seren Lanza,‡ Joseph Horwitz,|| and Ernest M. Wright‡

Departments of Physiology and Pathology, and Ophthalmology, Jules Stein Eye Institute, David Geffen School of Medicine at UCLA, Los Angeles, California 90095-1751

Received October 21, 2005; Revised Manuscript Received December 8, 2005

ABSTRACT: The bacterial Na^+/galactose cotransporter vSGLT of *Vibrio parahaemolyticus* is a member of the sodium:solute symporter family (SSS). Previous studies using electron microscopy have shown that vSGLT is a monomeric protein. Computational and experimental topological analyses have consistently indicated that this protein possesses 14 transmembrane α-helices. Our previous study using attenuated total reflectance Fourier transform infrared spectroscopy (ATR-FTIR) to quantitate secondary structure content had indicated, in contrast, an α-helical content of only 35%, too little to be consistent with the 14-span model [le Coutre, J., et al. (2002) *Biochemistry 41,* 8082−6]. ATR-FTIR had also indicated that upon binding of Na^+ and D-galactose, the α-helical content increased to 53%. Here we revisit the vSGLT secondary structural distribution using an alternative approach, ultraviolet circular dichroism spectropolarimetry (CD), which is highly accurate in determining the α-helical content of a protein in solution. CD spectra were obtained from actively functional, soluble vSGLT and, as an internal check, from a fusion protein of vSGLT and the *β*-barrel green fluorescent protein (GFP). Far-UV CD of vSGLT indicates a predominating 85% α-helical content, and an absence of *β*-strands. Far-UV CD of the vSGLT−GFP fusion corroborates this profile, indicating an equivalent α-helical content, and a *β*-strand content consistent with the GFP contribution. No detectable substrate-induced macroscopic changes in secondary structure are apparent in the far UV. In the near UV, increases in positive CD intensity occur in a stepwise manner with added substrates, implying changing environments of aromatic amino acid residues. CD thus confirms the current 14-transmembrane span model of vSGLT and reveals distinct substrate-induced conformational changes. The high percentage of α-helical structure found requires, when considered in the context of membrane topology, that nearly a third of the total α-helical fraction lies in extramembrane domains, which distinguishes this cotransporter from the unrelated lactose and glycerol 3-phosphate transporters.

Cotransporters drive the import of metabolites into cells through coupling to cation transport. The sodium:solute symporter family (SSS)[1] includes more than 700 sequences (*1, 2*). The *Vibrio parahaemolyticus* Na^+/galactose cotransporter, vSGLT, is an accessible model of SSS cotransporter function. Previous work has shown that both vSGLT and the human isoform SGLT1 are fully functional as monomers (*3, 4*). The topology of human SGLT1, determined by N-linked glycosylation scanning mutagenesis and corroborated by several computational algorithms, indicates SGLT1 consists of an extracellular N-terminus which precedes 14 transmembrane spans (*5*). This basic structural motif has since been found experimentally to be common to three homologues of human SGLT1: rabbit SGLT1 (14 spans), the rat Na^+/iodide symporter NIS (13 spans), and the *Escherichia coli* Na^+/proline transporter PutP (13 spans) (*6*−*9*).

We previously employed ATR-FTIR to examine vSGLT secondary structure, using active, reconstituted proteoliposomes dried on a germanium internal reflection element (*10*). This technique indicated an increase in the α-helical fraction from 35% in K^+ to 53% in the presence of Na^+ and D-galactose, with a corresponding decrease in the extent of hydrogen−deuterium exchange. The reproducible, surprisingly large, substrate-induced changes in secondary structure are puzzling, and the low, 35% α-helical content is difficult to square with the secondary structure model of 14 transmembrane spans.

To resolve these questions, here we have utilized circular dichroism (CD), a method recognized for its particular accuracy in determination of the α-helical content of proteins (*11*). Notably, CD structural analysis is currently experienc-

† Supported by NIH Grants DK19567 and DK44602. The Microsequencing Core Facility, Beckman Research Institute of the City of Hope, was funded by NIH Cancer Center Support Grant CA33572.

* To whom correspondence should be addressed: Department of Physiology, David Geffen School of Medicine at UCLA, Los Angeles, CA 90095-1751. Telephone: (310) 825-6968. Fax: (310) 206-5886. E-mail: eturk@mednet.ucla.edu.

‡ Department of Physiology, David Geffen School of Medicine at UCLA, University of California.

§ Department of Pathology, David Geffen School of Medicine at UCLA, University of California.

|| Department of Ophthalmology, Jules Stein Eye Institute, University of California.

[1] Abbreviations: ATR-FTIR, attenuated total reflectance Fourier transform infrared spectroscopy; C12M, dodecyl *β*-D-maltoside; CD, circular dichroism; DSSP, algorithm for secondary structural fractions from crystallographic data; GFP, green fluorescent protein; nrmsd, normalized root-mean-square deviation; RSD, relative standard deviation; SSS, sodium:solute symporter family.

10.1021/bi052160z CCC: $33.50
Published on Web 01/11/2006

ing a renaissance, due primarily to increased computational accuracy which in turn is based upon the current availability of many more determined protein crystallographic structures (*12*−*14*).

As CD spectra of membrane proteins in liposomes can be subject to artifacts from light scattering and band flattening, we chose to study detergent-solubilized vSGLT. The functional integrity of the soluble protein was established using a fluorescence assay (*15*). Analysis of the far-UV CD spectrum of vSGLT reveals a protein of high, 85%, α-helical content, which fully supports the 14-transmembrane span model. A fusion protein of vSGLT and *β*-sheet-rich GFP served as a check in evaluating the reliability of vSGLT CD analysis. Although ligands did not alter the far-CD spectra of vSGLT, we detected changes in the near-UV CD consistent with substrate-induced conformational changes. Possible explanations for the differences in the interpretation of the ATR-FTIR and CD spectra of vSGLT are discussed.

METHODS

Design and Expression of vSGLT Fusion Constructs 3C423 and VNGFPH6. Two vSGLT constructs were studied by CD spectropolarimetry: (1) construct 3C423 (Figure 1), which in addition to the 14 native transmembrane spans has an introduced 15th (from human glycophorin A) appended C-terminally, to place the C-terminal hexahistidine tag within the cytoplasm, and (2) construct VNGFPH6 (Figure 1), which has 15 spans such as 3C423, and a C-terminal GFP fusion (green fluorescent protein). The cysteine-less version of 3C423 displays 122% of the Na^+-D-galactose uptake activity of wild-type vSGLT in JM1100 cells (*16*) and 11−20-fold greater activity than the 14-span construct VNH6A (Figure 1) which had been used previously for ATR-FTIR (*10*). Cells expressing VNGFPH6 exhibited, in different cell cultures, from 20 to 102% of the uptake activity of wild-type vSGLT.

Construct 3C423 has, in addition to the glycophorin span, an introduced cysteine residue, A423C, and a C411A mutation which removes the sole native cysteine (*15*). Construct VNGFPH6 is a fusion protein of (a) wild-type vSGLT (GenBank accession number P96169) fused to (b) the 15th transmembrane span as in 3C423, fused to (c) the green fluorescent protein GFP_{UV} variant (*17*), and terminates in (d) a hexahistidine tag (*4*). The cytoplasmic GFP moiety is fluorescent and, hence, properly folded.

The coding sequences for all constructs were placed under the control of the pBAD promoter (*4*). All constructs were sequenced to ensure fidelity. Expression of construct proteins was induced constitutively with 20 *μ*M L-arabinose in overnight cultures at 30 °C in LB medium.

Protein Purification. The protein of each vSGLT construct was expressed in *E. coli* strain XL1-Blue (Stratagene) from a pBAD18 plasmid vector by constitutive induction overnight in 20 *μ*M L-arabinose in LB medium at 30 °C. The His-tagged protein constructs were purified by nickel chelate and gel filtration chromatography (*4*). The purified protein was kept at 4 °C in a detergent solution containing 0.5 mM D-galactose, 200 mM NaCl, and 12% glycerol and did not aggregate in storage.

Preparation of Protein Samples for CD Spectropolarimetry and Fluorometry. Purified 3C423 or VNGFPH6 protein was exchanged into buffer B containing 6 mM K_2HPO_4, 4 mM KH_2PO_4, 20 mM KCl, and 0.02% dodecyl *β*-D-maltoside (C12M) (pH 7.2) by using a Microcon YM-50 centrifugal ultrafiltration device (Millipore). Particulates were removed by centrifugation at 15000*g*. Positive displacement pipettors (Rainin, Woburn, MA) were used exclusively to ensure high accuracy and reproducibility of volumes. The protein was added to buffer B containing the test cation (K^+ or Na^+ sulfate) and the test sugar (D-galactose or L-glucose) at concentrations of 200 mequiv of K^+/L or 200 mequiv of Na^+/L, with 0−20 mM sugar and 0.4 mg/mL protein. The A_{280}/A_{260} UV absorbance ratio of 3C423 was 1.81, indicating essentially no nucleic acid contamination.

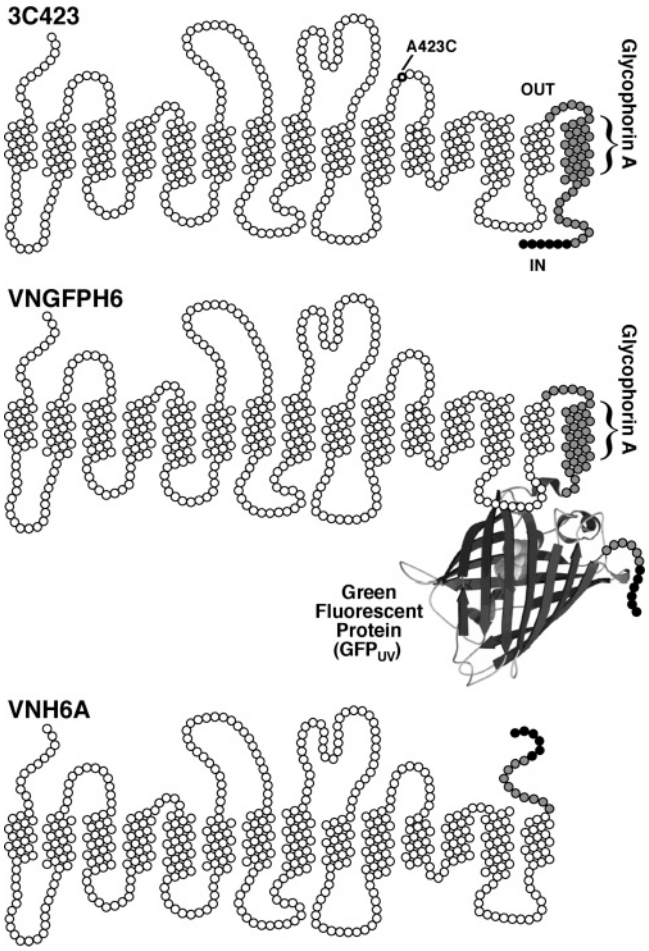

FIGURE 1: Secondary structure models of three vSGLT constructs. The hexahistidine sequence used for purification is highlighted in black, and other residues appended to the native vSGLT C-terminus are colored gray. The VNH6A construct was used in a related ATR-FTIR study, and not here. It has 14 native transmembrane spans and a periplasmic orientation of the hexahistidine tail. Construct 3C423 incorporates a 15th transmembrane span from human glycophorin A to reorient the hexahistidine tail to the cytoplasm. The A423C mutation is its only Cys residue, which was used for fluorescent labeling to demonstrate substrate-induced functional conformational changes in detergent. Construct VNGFPH6 has a *β*-strand-rich green fluorescent protein domain appended to the 15th transmembrane span.

Assessment of 3C423 Functional Integrity by Fluorescence Quenching. Fluorescence measurements of 3C423 labeled with the maleimide ThioGlo-3 (Covalent, Woburn, MA) at Cys423 were taken on a Fluorolog-3 spectrofluorometer (*15*). ThioGlo-3 (final concentration of 5−15 *μ*M) was added to 620 nM 3C423 (40 *μ*g/mL) in 120 *μ*L of 50 mM potassium

phosphate (pH 7) (*15*). Fluorescence emission was recorded after labeling was complete (15−20 min) at 443 nm, with excitation at 363 nm. The $K_{0.5}$ for D-galactose was determined from the extent of fluorescence quenching of ThioGlo3-labeled 3C423 with an increase in D-galactose concentration in the presence of 200 mequiv of Na^+/L (phosphate counterion); an increasing concentration of L-glucose, a nontransported sugar, served as a control. The $K_{0.5}$ for Na^+ was similarly determined by increasing the Na^+ concentration in the presence of 20 mM D-galactose; an increasing K^+ concentration served as a control.

Determination of Protein Concentrations for CD Analysis. Accurate protein quantitation is critical to CD analysis. Standard colorimetric methods failed for accurate measurement of vSGLT, due to irreversible protein aggregation after precipitation with either chloroform and methanol or trichloroacetic acid, in attempts to remove interfering solutes. High variability and spuriously low estimates of protein content resulted from subsequent quantitation by either amino acid analysis or bicinchoninic acid assay (BCA).

The spectroscopic protein quantitation method of Waddell (*18*) was ultimately found to be accurate and insensitive to the solutes in vSGLT samples, thereby circumventing the need for precipitation. A proportionality constant, C, relates the difference in absorbance at two wavelengths to protein concentration

$$[\text{protein}]\ (\text{mg/mL}) = C(A_{215} - A_{225}) \qquad (1)$$

where A_{215} and A_{225} are sample absorbance values corrected for buffer absorbance. Peptide bond UV absorbances on the steep upslope at 215 and 225 nm are nearly independent of protein amino acid composition. By taking the difference between these two absorbances, we minimize the potential interference from light scattering and background variability. These three features, together with several-fold greater sensitivity, distinguish this method from the common measurement of tryptophan/tyrosine absorbance at the single wavelength of 280 nm. Estimates of C were determined for the two vSGLT proteins using total amino acid analysis. The values ($C_{3C423} = 0.137$ and $C_{VNGFPH6} = 0.148$) were within 5% of the value reported for the total serum protein (0.144).

For total amino acid analysis, a 30−40 μL aliquot of the protein sample used for CD was added to 50 μL of dialysis buffer (5 mM $NH_4{\cdot}HCO_3$ and 0.02% Triton X-100) in a Mini Dialysis unit (Pierce Biotechnology). Dialysis proceeded overnight against 1 L of dialysis buffer. The retentate was transferred to a glass hydrolysis tube, dried under vacuum, and hydrolyzed above 6 N HCl at 110 °C in argon for 24 h. The hydrolysate was dried and dissolved in 200 μL of water. Amino acid analysis was carried out at the Microsequencing Core Facility, Beckman Research Institute of the City of Hope, Duarte, CA. The mix of 17 amino acids used as a standard was Standard Reference Material 927c (National Institute of Standards and Technology, Gaithersburg, MD). The bovine serum albumin standard was at 71.57 ± 0.74 g/L (Standard Reference Material 2389). The test samples and triplicate samples of 0.40 μg of BSA standard were hydrolyzed simultaneously. Underivatized amino acids of the hydrolyzed standard or test samples were resolved by HPLC on a Dionex AAA-Direct column and detected by pulsed amperometry. The integrated peak values of Standard Reference Material 2389 were used to determine the percentage recovery of hydrolyzed BSA standard, from the known amino acid composition of BSA. The recovery was then used to correct the integrated peak values of the hydrolyzed test samples. The known amino acid sequences of the vSGLT constructs were used with the corrected integrated peak values to calculate their protein concentrations. Duplicate samples agreed to within 0.5%.

Circular Dichroism and Secondary Structural Analysis. CD spectra were recorded at 22 °C on a Jasco J-810 spectropolarimeter. For far-UV measurements, a quartz cell with a path length of 0.2 mm was used, and each final spectrum was the average of 16 scans from 260 to 190 nm. Protein concentrations in milligrams per milliliter were typically 0.38 (3C423) and 0.40 (VNGFPH6). Near-ultraviolet CD spectra of 3C423 (0.49 mg/mL) were recorded using a 1 cm path length cell, and each final spectrum was the average of 32 scans from 320 to 250 nm.

CD spectra were analyzed for the content of secondary structure fractions using CDPro and its suite of three algorithms: CONTINLL, CDSSTR, and SELCON3 (*12*). These programs are based upon a locally linearized ridge regression method (CONTINLL), and the self-consistent method using the singular-value decomposition algorithm (CDSSTR and SELCON3). Each program utilizes a unique strategy and differing constraints and criteria to select the best set of calculated structural fraction values. The protein reference set used was SMP56, which includes 13 transmembrane and 43 soluble proteins (*13*). Final estimates of secondary structure fractions were taken as the average of corresponding fraction values calculated by CDSSTR and CONTINLL. The normalized root-mean-square deviation (nrmsd) was used as a measure of the goodness of fit between the experimental spectrum and the curve calculated from the crystallographic data in SMP56. The nrmsd for a calculated curve is expressed as

$$\text{nrmsd} = \sqrt{\frac{\sum_N (\Delta\epsilon_{\text{exptl}} - \Delta\epsilon_{\text{calc}})^2}{\sum_N (\Delta\epsilon_{\text{exptl}})^2}} \qquad (2)$$

where $\Delta\epsilon_{\text{exptl}}$ and $\Delta\epsilon_{\text{calc}}$ are the experimental and calculated dichroic molar absorption per amino acid residue, respectively, and N is the number of data points (*19*).

Calculation of the Number of α-Helices and β-Strands. Because of differences in H-bonding, the dichroism of peptide groups at the ends of an α-helix (called "distorted") differs from that of the internal remainder of the α-helix. The total number of α-helical segments, N_α, can be estimated from the distorted fraction:

$$N_\alpha = \frac{N_{aa} H(d)}{4} \qquad (3)$$

where N_{aa} is the total number of amino acid residues in the protein, $H(d)$ is the calculated distorted α-helical fraction, and 4 reflects an empirical value of two distorted peptide groups at each end of an α-helical segment (*20*). The number

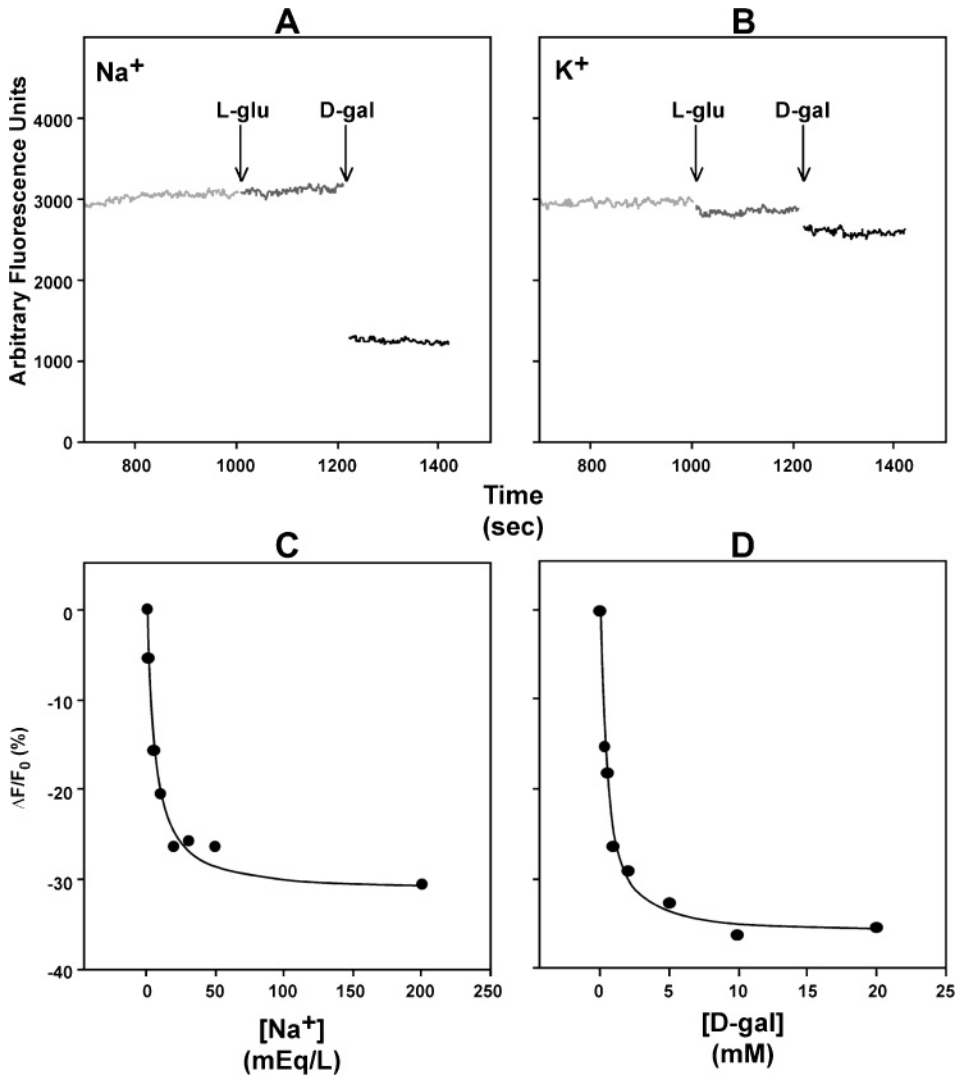

FIGURE 2: Binding of substrates quenches the fluorescence of detergent-solubilized vSGLT construct 3C423. (A and B) 3C423 in 0.02% dodecyl β-D-maltoside was fluorescently labeled at Cys423 by preincubation for 800 s with 5 μM ThioGlo-3 in either 200 mequiv of Na^+/L or 200 mequiv of K^+/L, with phosphate counterion; L-glucose or D-galactose was then added to a final concentration of 20 mM at the indicated times. (C) Effect of increasing Na^+ concentrations on the fluorescence in 20 mM D-galactose. (D) Effect of increasing D-galactose concentrations on the fluorescence in 200 mequiv of Na^+/L. The apparent affinity (K_d) and saturated quench ($\Delta F_{satn} = F_0 - F_{satn}$) were derived by nonlinear curve fitting of the equation $\Delta F/F_0 = (\Delta F_{satn}/F_0)[S]/(K_d + [S])$ to the quench vs concentration plot. Note that the studies depicted in panels A and B were carried out with protein samples different from those used for panels C and D.

of β-strands was estimated by an analogous equation, using the empirical value of 2 distorted peptide groups per β-strand (*20*).

RESULTS

Conformational Activity of 3C423 in Detergent Mixed Micelles. vSGLT construct 3C423 in detergent was selected for these studies because this construct permits the recording of CD spectra and the determination of functional activity of the same protein sample. The function of 3C423 vSGLT in detergent was assayed by measurement of Na^+-dependent D-galactose quenching of fluorescence of ThioGlo-3-labeled 3C423 (*15*). Labeled 3C423 in 200 mequiv of Na^+/L showed an immediate 41% quench of emission upon addition of 20 mM D-galactose but no quench with the nonbinding sugar 20 mM L-glucose (Figure 2A). This D-galactose-specific effect was essentially absent in K^+ buffer (Figure 2B). In 200 mequiv of Na^+/L (Figure 2D), the quench induced by D-galactose was concentration-dependent and saturable, with an apparent D-galactose K_d of 0.42 mM. Likewise, in 20 mM D-galactose, the quench was a saturable function of the Na^+ concentration (Figure 2C), with an apparent Na^+ K_d of 5.2 mequiv/L. These K_d values are indistinguishable from those obtained for 3C423 vSGLT reconstituted in proteoliposomes (*15*), showing that the cotransporter retained its functionality, and its associated repertoire of native conformations, in detergent micelles.

3C423: Circular Dichroism in the Far UV. CD spectra of detergent-solubilized 3C423 were obtained under five different substrate conditions with sulfate as the counterion: (a) 200 mequiv of K^+/L, (b) 200 mequiv of K^+/L and 0.48 mM D-galactose, (c) 200 mequiv of Na^+/L, (d) 200 mequiv of Na^+/L and 0.48 mM D-galactose, and (e) 200 mequiv of Na^+/L and 0.48 mM L-glucose. The dodecyl β-D-maltoside detergent (C12M) contributed negligibly to the background UV absorption and light scatter. The profiles of the five CD spectra of 3C423 (Figure 3) were essentially superimposable, with no visible differences among the five substrate condi-

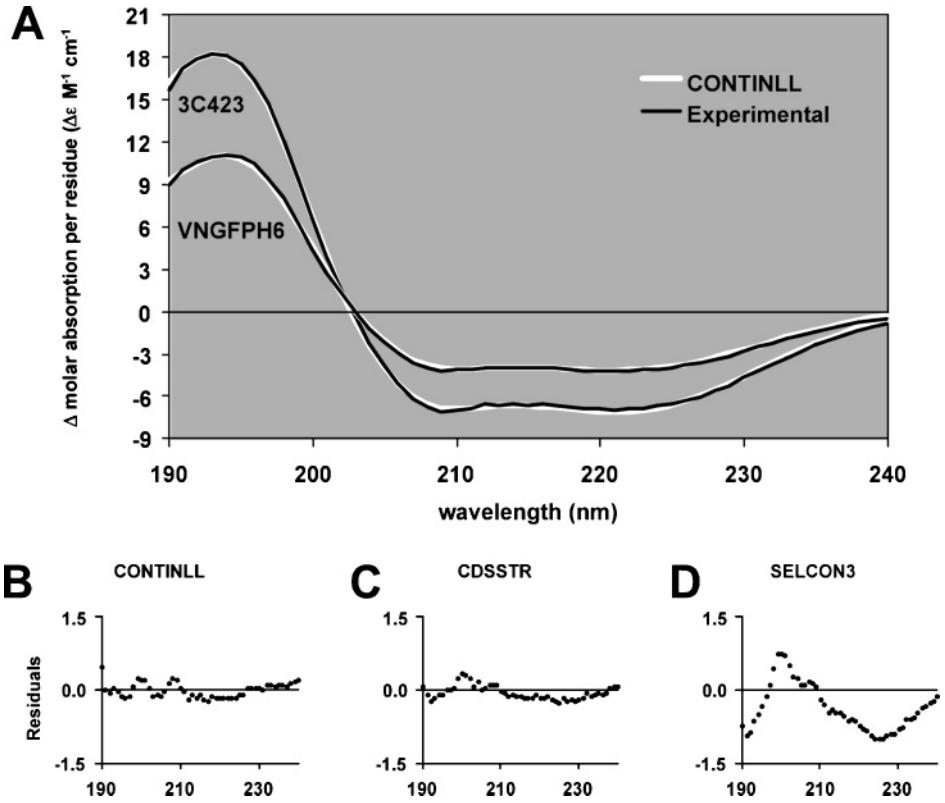

FIGURE 3: Far-UV CD spectra of 3C423 and VNGFPH6 and derived curves calculated by CONTINLL. (A) The CONTINLL-calculated curves conform well to the experimental spectra of 3C423 and VNGFPH6. CDSSTR-calculated curves (not shown) were essentially identical to those of CONTINLL. (B−D) The 3C423 residuals of the CONTINLL and CDSSTR curves are small, but those of SELCON3 are significantly greater and indicate the broad regions where the SELCON3 curve deviated persistently from the experimental results.

Table 1: Secondary Structure Fractions Determined from CD Spectra

		α-helix (%)[a]			β-strand (%)[b]					
vSGLT construct	program	*H*(r)	*H*(d)	Σ*H*	*S*(r)	*S*(d)	Σ*S*	% turn	% unordered	nrmsd
3C423	CONTINLL	58	24	82	0.2	0.1	0.3	4.5	14	0.019
	CDSSTR	62	28	89	1.6	−1.0	0.7	2.8	5.9	0.019
VNGFPH6	CONTINLL	39	20	59	4.1	3.5	7.5	12	22	0.022
	CDSSTR	39	21	60	4.9	3.5	8.4	11	20	0.035

[a] *H*(r) is for regular α-helix (α-helix peptide groups other than the two at each α-helix end). *H*(d) is for distorted α-helix (two α-helix peptide groups at each end of each α-helix). $\Sigma H = H(r) + H(d)$. [b] *S*(r) is for regular β-strand (β-strand peptide groups other than the ones at each β-strand end). *S*(d) is for distorted β-strand (one β-strand peptide group at each end of each β-strand). $\Sigma S = S(r) + S(d)$.

tions. The spectra cross the zero ellipticity axis between 202 and 203 nm, and two minima appear at 221 and 209 nm, typical of an α-helix-rich protein. Positive ellipticity is maximal at 193 nm. The $\Delta\epsilon_{221}/\Delta\epsilon_{209}$ ratio is 0.98; a ratio near 1 is characteristic of α-helices that closely interact, such as coiled-coil α-helices (*21*, *22*).

Five 3C423 spectra, one for each of five substrate conditions, were analyzed for secondary structure content using the CDSSTR and CONTINLL algorithms (*12*). (Despite algorithm SELCON3's general agreement with the curves calculated by these two algorithms, it was not used for reasons discussed below.) Each spectrum represented the averaged composite of 16 tandem scans.

These five spectra were essentially superimposable, with no apparent dependence on substrate conditions. As with the five originating experimental spectra, the five derived curves were also essentially superimposable. Therefore, to fully utilize all spectral data that were collected, the five spectra were averaged together to form one composite experimental spectrum (Figure 3A). Similarly, the calculated curves produced two averaged composite curves, one each from CDSSTR (not shown) and CONTINLL (Figure 3A). The composite CDSSTR and CONTINLL curves made excellent fits with the composite experimental spectrum, as indicated by the residuals, $\Delta\epsilon_{experimental} - \Delta\epsilon_{calculated}$ (Figure 3B,C). The average value of the normalized root-mean-square deviations (nrmsd, eq 2) of the five CONTINLL and five CDSSTR curves, calculated for each 3C423 experimental spectrum, was 0.019; an nrmsd value of ≤ 0.1 indicates excellent agreement between the experimental and calculated curves (*19*, *23*).

Secondary structure fractions of 3C423 were calculated from each of the five substrate-specific experimental spectra, and each fraction was averaged: the relative standard deviations (RSD) were <1%. The total α-helical fraction calculated by CONTINLL (82%) and CDSSTR (89%) gives an average value of 85 ± 5% α-helix (Table 1). Both programs indicated less than 1% β-strand (i.e., fewer then six amino acid residues, or fewer than three H-bonds), an average turn fraction of 4 ± 1%, and an average unordered

Table 2: Derived Values of the Number of α-Helices, β-Strands, and Amino Acid Residues in Structure Fractions

			α-helix[a]					β-strand[b]	
vSGLT construct	program	no. of amino acid residues	$\sum H$(r,d) (%)	N_α	AA_α	$AA_{\alpha-ms}$	$AA_{\alpha-aq}$	N_β	AA_β
3C423	CONTINLL	593	82	35	485	355	130	0.4	2
	CDSSTR		89	41	530		175	(−2.8)	(4)
VNGFPH6	CONTINLL	827	59	41	485	355	130	14	62
	CDSSTR		60	43	495		140	14	69
(GFP)	CONTIN[c]	238	20	−	48	−	−	−	124
	CONTINLL[d]		5	3	11	−	−	15	98
	CDSSTR[d]		7	4	16	−	−	16	79
	(DSSP)[e]		2	1	4	−	−	11	118

[a] $\sum H$ is the percentage total calculated α-helix fraction = %H(r) + %H(d). N_α is the total number of calculated α-helical segments. N_α = (total number of amino acid residues) × H(d)/(4 distorted residues/α-helix). AA_α is the number of amino acid residues in the calculated α-helix fraction. $AA_{\alpha-ms}$ is the number of amino acid residues in membrane-spanning α-helices and was estimated from the sum of 28 residues in the glycophorin A span plus the residues delimited by spanning helix ends of vSGLT as determined by the interfacial hydrophobicity/reverse turn propensity method IFH/RT (*2*, *26*). $AA_{\alpha-aq}$ is the number of residues in non-membrane-spanning α-helices = $AA_\alpha - AA_{\alpha-ms}$. [b] N_β is the number of calculated β-strands. N_β = (total number of residues) × H(d)/(2 distorted residues/β-strand). AA_β is the number of amino acid residues in the calculated β-strand fraction. [c] Experimental data of Visser et al. (*35*) as originally analyzed using a data set of 16 soluble proteins (*47*). [d] Experimental data of Visser et al. (*35*) reanalyzed using the SMP56 data set (*13*). [e] "Actual" GFP secondary structure fraction values derived from crystallographic data (*27*).

structure fraction of 10 ± 5%. From the distorted α-helix fraction, it may be estimated that there are between 35 and 41 α-helical segments in 3C423 (Methods and Table 2).

VNGFPH6: Circular Dichroism in the Far UV. CD spectra of VNGFPH6, a fusion protein of vSGLT and GFP, were recorded under the same five substrate conditions used for 3C423, and these were also found to be superimposable; therefore, all were used for CD analysis as an averaged composite spectrum as described above. The composite CD spectrum (Figure 3A) is characterized by an overall reduction in intensity relative to that of 3C423, which is consistent with "dilution" of the primarily α-helical vSGLT structure with the nonhelical, β-barrel GFP structure. The minimum at 209 nm is ∼40% less intense than that of 3C423; the ratio of the minima is slightly greater ($\Delta\epsilon_{222}/\Delta\epsilon_{209} = 1.02$), and the positive maximum is red-shifted relative to that of 3C423 by ∼1 nm, to 194 nm. These changes are consistent with expected consequences of the introduction of GFP β-sheets. The CONTINLL- and CDSSTR-calculated curves conform closely to the experimental spectrum (Figure 3A), showing low nrmsd values of 0.022 and 0.035 (Table 1).

The VNGFPH6 α-helical fraction values calculated from the five substrate-specific spectra by CONTINLL or CDSSTR averaged 59−60% with RSDs of <1% (Table 2). Each program significantly underestimated the actual (14%) β-strand fraction contributed by the GFP domain, 7.5% by CONTINLL and 8.4% by CDSSTR, with RSDs of 4 and 18%, respectively. The turn fraction was calculated at 11−12% and the unordered fraction at 20−22%, both with RSDs of ≤6%. The number of α-helices in VNGFPH6 was estimated from the distorted α-helical fraction to be 41−43 (Methods and Table 2).[2]

[2] SELCON3 analysis of 3C423 indicated an α-helical content of 90% and an absence of β-strands. Although the SELCON3 nrmsd was an otherwise acceptable value of 0.07, the residuals ranged up to ±1.1 molar absorption units per residue, as graphed in Figure 3D, and the calculated curve deviated persistently from the experimental curve. For VNGFPH6, SELCON3 calculated an α-helical content of 57% and generated a curve that again deviated persistently from the experimental spectrum and had a relatively high nrmsd of 0.105. Therefore, SELCON3 results were not used in the structural analyses of either 3C423 or VNGFPH6.

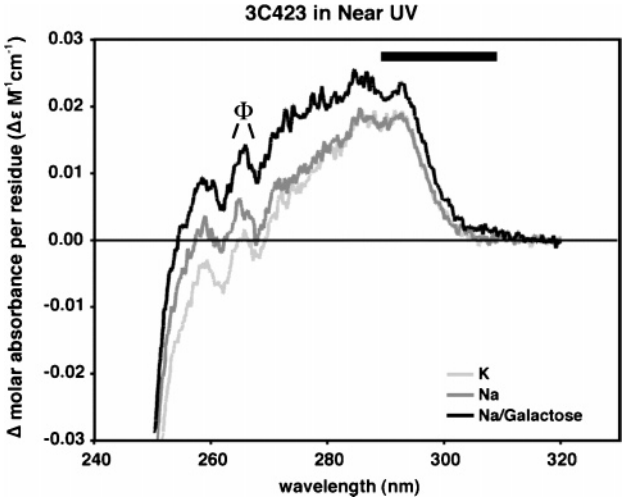

FIGURE 4: Increased near-UV dichroism of aromatic residues of 3C423 induced by the addition of substrates. 3C423 spectra were recorded in buffer B containing (i) 200 mequiv of K^+/L, (ii) 200 mequiv of Na^+/L, or (iii) 0.48 mM D-galactose and 200 mequiv of Na^+/L, with sulfate counterion. The horizontal line indicates positive dichroism of the tryptophan L_b band. Phenylalanine contributions to negative dichroism at 262 and 268 nm are indicated by Φ.

3C423: Circular Dichroism in the Near UV. CD spectral contributions from tryptophan, tyrosine, and phenylalanine were recorded in the near UV between 320 and 250 nm. The peak at 292 nm in the absence of substrates indicates that positive dichroism of the tryptophan L_b band dominates the spectrum (Figure 4). Phenylalanine contributions to negative dichroism are evident in the peaks at 262 and 268 nm; the first Phe fine structure band is typically near 270 nm (*24*, *25*). Relative to the spectrum in 200 mequiv of K^+/L, a small increase in intensity extending below 283 nm appeared in 200 mequiv of Na^+/L and increased with decreasing wavelength.

A further increase in intensity, but now extending below 309 nm, occurred in Na^+ with 0.48 mM D-galactose. A careful measurement of the UV absorbance curve was recorded simultaneously with acquisition of each CD spectrum. The three absorbance spectra were superimposable, indicating that the intensity changes noted among the three

CD spectra did not derive from differences in scatter, background, or sample variability.

Estimation of the Extrabilayer Subfraction of α-Helical Amino Acid Residues. The total α-helical fraction can be subdivided into (a) α-helices participating in membrane spans and (b) α-helices in nonbilayer domains. These were derived as follows. Using the experimentally and computationally determined transmembrane α-helical regions of SGLT1 as a starting point, the putative ends of homologous vSGLT membrane spans were estimated by an interfacial hydrophobicity/reverse turn propensity method, IFH/RT (*26*), which had been applied previously to human SGLT1 and lactose permease (*2*, *5*). The number of lactose permease residues in transmembrane α-helices as found by crystallography is within 5% of the IFH/RT estimate, an indication of suitable accuracy. IFH/RT analysis of vSGLT (not shown) indicates 327 amino acid residues in membrane spans, averaging 23−24 residues per span, consistent with bilayer thickness. 3C423 has an additional (15th) transmembrane span comprised of the 28-residue glycophorin α-helix, yielding ∼355 residues in transmembrane α-helices. Thus, from 130 to 175 residues, or 27−33% of the total α-helical fraction, are implied to occur in nonbilayer α-helices (Table 2).

An estimate of the number of α-helical segments, N_α, can be derived from the distorted α-helical fraction. N_α was calculated to be 35−41 for 3C423, agreeing well with the value of 41−43 similarly obtained for VNGFPH6, which incorporates one additional α-helix of four residues. The factor of $^1/_4$ in eq 3 was originally tailored such that CD-derived estimates of N_α best matched the N_α values derived by DSSP (*27*) from the crystallographic structures of the proteins in CD reference set SMP56. However, it should be noted that by using the protein structure visualization program Swiss-PdbViewer (*28*), it is apparent that DSSP yields a greater number of transmembrane α-helices than is apparent to the eye, a result of subtle bends and kinks in otherwise continuous helices. For example, lactose permease has 12 α-helical transmembrane domains, while DSSP partitions these into 19 α-helical segments.

DISCUSSION

Our previous ATR-FTIR study of the *Vibrio* Na/D-galactose cotransporter vSGLT indicated a low α-helical content inconsistent with the topological model of 14 transmembrane α-helical spans (*5*, *10*). The secondary structure content of vSGLT was therefore reevaluated by CD spectropolarimetry, a fundamentally different physical technique whose particular strength is the accurate estimation of α-helical content.

The secondary structural profiles of vSGLT that were indicated by CD and by FTIR were so disparate that several stringent measures were taken to ensure high CD accuracy.

(i) Protein concentrations were estimated using an accurate and robust UV absorption difference method. We standardized eq 1 for each construct, based upon amino acid analysis (Methods).

(ii) Structural quantitation by CD is fundamentally dependent upon the accuracy of the estimate of protein concentration. The volume accuracy of detergent solution aliquots is inherently low for air displacement pipets due to tip wettability; therefore, positive displacement pipettors were used exclusively to ensure accurate protein concentrations.

(iii) The soluble form of vSGLT was functionally active. Substrate-dependent conformational changes in vSGLT were demonstrated in proteoliposomes by fluorescence quenching of labeled 3C423 (*15*). 3C423 in detergent micelles also shows this substrate-specific quench, with K_d values for Na^+ and D-galactose that are essentially indistinguishable from those obtained in cotransport-competent proteoliposomes. Evidently, vSGLT retains its functional activity in C12M detergent.

(iv) The use of detergent-solubilized protein avoids scattering and band flattening artifacts associated with membranes (*29*, *30*).

(v) A large crystallographic reference set of protein basis spectra was utilized. The prior lack of a CD database that includes membrane proteins has been cited to compromise structural accuracy for membrane proteins (*14*). This issue was addressed by introduction of the SMP56 reference set, which incorporates data on nine α-helical membrane proteins (*13*).

(vi) CD-derived estimates of secondary structure content were cross-checked by utilizing three independent computer algorithms.

(vii) The CD-derived decrease in relative α-helical content which results from fusing GFP to 3C423 (VNGFPH6 construct) is consistent with the calculated value, accounting for the secondary structure contributions of GFP, as determined from crystallography.

The algorithms supplied with the CDPro CD analysis package (*12*) were used to analyze the far-UV CD spectrum of 3C423. CONTINLL, CDSSTR, and SELCON3 indicated that the *Vibrio* vSGLT Na^+/D-galactose cotransporter has no β-strands and is a primarily α-helical structure with 82, 89, and 90% α-helix, respectively. The averaged CONTINLL and CDSSTR values for other fractions were 3.6 ± 1.2% turns and 9.7 ± 5.4% unordered structure (Table 1). CONTINLL and CDSSTR analyses of 3C423 gave the low nrmsd value of 0.019, and their calculated curves conformed closely to the experimental spectrum (Figure 3A−C). The calculated fraction of total α-helix was not overly sensitive to potential errors in the determination of protein quantity; a hypothetical error of ±5% in estimated protein concentration resulted in a 3−4% change by either program.

The secondary structural profile of vSGLT that results is that of a largely α-helical protein devoid of β-sheets. This profile parallels that of two transporters in the functionally related major facilitator superfamily (*31*). Crystallographic analyses of the lactose permease and the glycerol 3-phosphate antiporter (GlpT) reveal 80 and 74% α-helical structures and a complete lack of β-sheets (*32*, *33*). In contrast to the CD of lactose permease and GlpT, the CD of 3C423 indicates that a large fraction of its total α-helical content resides in nontransmembrane domains: ∼30%, vs 5% for lactose permease or GlpT (see below). The greater nonbilayer α-helical content of vSGLT is consistent with its larger number of extramembrane residues (∼238 vs 102 in lactose permease, 140 in GlpT).

The legitimacy of the CD secondary structure values obtained for 3C423 was examined by appending a protein of known structure. The GFP moiety of construct VNGFPH6 (Figure 1) is β-rich and contributes one four-residue α-helix. Its calculated α-helical content should therefore closely match that of 3C423. Preparations of VNGFPH6 are

intensely green fluorescent; the GFP moiety is thus folded into its native β-barrel structure. CONTINLL and CDSSTR calculated the equivalent of 485−495 amino acid residues in the total α-helix fraction, in agreement with the range of 485−530 calculated for 3C423 (Table 2), despite the greater size and complexity of VNGFPH6. The addition of a large β-rich structure (GFP) had evidently little effect on the calculation of the α-helical fractions, although both programs underestimated the β-strand content (79−98 amino acid residues vs 118 actual, Table 2). The large contribution of vSGLT α-helical structure to the total ellipticity of VNGFPH6 may be expected to partially mask the weaker β-strand contribution. Underestimation of the β-strand content is consistent with the significantly lower accuracy of all CD algorithms in determining the β-strand fractions (*12*, *13*). Both programs overestimated the number of β-strands (14 vs 11 actual) [PDBFINDER database (*34*)], but the difference of three strands falls within the range of errors reported for CD estimates of β-strands for 29 proteins of known crystallographic structure (*20*).

A previously published CD analysis of GFP (*35*) estimated the β-strand content to be 52%, close to the actual value of 50%, but significantly overestimated the α-helical fraction (20% vs <2%). A reanalysis of that data via CONTINLL and CDSSTR and the SMP56 reference set (Table 2) yields an improved estimate of 5−7% α-helix but less accurate estimates of β-strand content (33−41%).

This CD-derived profile of 3C423, 85 ± 5% α-helical content with an absence of β-sheets, more closely reflects the experimentally mapped topological structure of vSGLT than does the profile indicated by ATR-FTIR.

ATR-FTIR had indicated a 1.5-fold increase in the α-helical content of vSGLT upon addition of substrates. In contrast, five far-UV CD spectra of 3C423, each recorded under a different substrate condition, were superimposable, suggesting no changes occur in secondary structure content. We examined the near-UV CD spectrum of 3C423 to detect substrate-dependent conformational shifts affecting the environment of any of the 76 aromatic amino acid residues. In the absence of substrates, a positive tryptophan L_b band dichroism dominates, as evidenced by the peak at 292 nm (Figure 4). This indicates a prominent contribution from tryptophans in hydrophobic environments. Nine of the 3C423 tryptophans are indicated in the secondary structure model to reside within the membrane, which is consistent with both the dominating L_b type of CD band and the blue-shifted tryptophan fluorescence emission peak seen at 327 nm (*36*). Relative to CD in K^+, dichroism below 283 nm increased in Na^+ as the wavelength decreased (Figure 4). CD difference spectra show no obvious vibrational band (data not shown). Dichroism increased further upon addition of D-galactose in Na^+, now extending to ∼309 nm. These dichroic increases indicate stepwise conformational shifts accompanying binding of ligands.

The CD intensity increase observed upon addition of D-galactose, seen extending up to 309 nm, indicates increased CD of the tryptophan L_a band, centered near 280 nm. Tryptophan is the only aromatic residue capable of absorbing up to and slightly beyond 309 nm, and its near-UV CD transition is especially sensitive to solvent accessibility and to the proximity and orientation of other aromatic side chains. The CD increase with D-galactose thus reflects conformational changes in the environment of one or more tryptophans. Tryptophan is commonly found to contribute to the binding site of sugar-binding proteins (*37*). It is conceivable that the dichroic increase with D-galactose reflects the direct influence of a bound D-galactose molecule on a binding-site tryptophan.

In the previous study, ATR-FTIR of vSGLT construct VNH6A (Figure 1) had indicated a minimum α-helical content of 35%, which increased to 53% in the presence of substrates (*10*). In contrast, CD analysis in the far UV indicates an 85% α-helix content that is invariable with ligands. It has been noted that the interpretation of protein FTIR data by curve fitting methods, like those we had employed, has a marked tendency to find 15−20% β-sheet content in α-helical proteins that are devoid of sheets (*38*, *39*). For example, the crystallographic structure of the membrane protein aquaporin 1 is predominantly α-helical (56%) with no β-strands, but two FTIR studies indicated 18 and 42% β-sheet structure content (*40*, *41*).

In ATR-FTIR, adsorption to the germanium surface has been observed to induce significant conformational changes in several proteins, producing multiple adsorbed conformational states, thus altering the IR spectrum (*42*). Such adsorption effects may be responsible for the anomalous ATR-FTIR estimates of vSGLT secondary structure. Adsorption phenomena may also account for the discrepancies noted between two earlier structural assessments of lactose permease: CD had indicated 85% α-helix, while ATR-FTIR had indicated 65% α-helix and 25% β-strand (*43*, *44*). Crystallography now demonstrates the permease has 86% α-helix and no β-sheets (*32*).

A possible explanation of the dramatic effects that substrate binding had on the FTIR spectrum of vSGLT follows. The ATR-FTIR experiments of Oberg and Fink (*42*) demonstrated that a fraction of protein molecules adsorbed to Ge equilibrates between an adsorbed, distorted state(s) and the nonadsorbed native state. Conformational changes in vSGLT accompany substrate binding, as evidenced by near-UV CD. (The change from K^+ to Na^+ resulted in a 60% increase in the absorption ratio, $A_{\parallel}/A_{\perp}$, of the ATR-FTIR amide II band of vSGLT, indicating a significant decrease in helical tilt relative to the Ge surface.) The considerable adsorptive structural distortion detected by ATR-FTIR would likely render the adsorbed state(s) of vSGLT incapable of binding substrate. By simple mass action, addition of Na^+ would shift the adsorbed ↔ nonadsorbed equilibrium toward two native, nonadsorbed forms: both unbound and Na^+-bound forms. Sugar would then shift the equilibrium further (i.e., toward unbound, Na^+-bound, and bound to Na^+ and sugar). (Additionally, the diminished rate and extent of H−D exchange seen in ATR-FTIR upon the addition of substrates indicated substrate-bound conformations of vSGLT to be more rigid and, thus, may themselves be more resistant to re-adsorption and deformation than unbound vSGLT.) The preceding scenario essentially describes a "conformational selection mechanism", which has been demonstrated in antibody/antigen recognition and leucine zipper formation (*45*, *46*). Whatever the mechanism, it is quite intriguing that conformational effects of substrate binding were somehow greatly magnified in ATR-FTIR; any plausible mechanism must account for the large magnitude of the change. It is not inconceivable that the

phenomenon, should it become physically well understood, may offer a new investigative tool.

In summary, far-UV CD reveals vSGLT to be a highly α-helical protein without β-strands, similar to the structural profiles of two crystallized, functionally related transporters of the major facilitator family. The use of the vSGLT single-Cys construct 3C423 in a detergent-solubilized form simplified CD spectral acquisition, essentially eliminated scattering and band flattening artifacts, and permitted CD acquisition and a functional assay on the same sample. The fluorescence quenching upon substrate binding demonstrates the solubilized 3C423 construct is conformationally active, not denatured, with ligand affinities indistinguishable from those measured in cotransporting proteoliposomes. Calculated CD curves closely conform to the experimental far-UV CD spectra with highly significant nrmsd values. Use of the large protein reference set SMP56 enhanced the accuracy of CD spectral analyses. The 85% α-helical content indicated by CD is fully consistent with the 14-transmembrane span topological model of native vSGLT that has extensive experimental support. CD analysis of a fusion of vSGLT to β-rich GFP as a control supported this estimate of α-helix content. Analysis of the CD data, coupled with IFH/RT predictions of transmembrane α-helix ends, indicates that a large fraction of the total α-helical content of vSGLT (27−33%) resides in its nonbilayer domains.

ACKNOWLEDGMENT

We thank Sophia Fong and Linlin Ding for technical assistance and Johannes le Coutre for helpful discussions. We also thank Hsiang-Hui (Betty) Meng for her generous help with the amino acid analyses.

REFERENCES

1. Wright, E. M., and Turk, E. (2004) The sodium/glucose cotransport family SLC5, *Pfluegers Arch. 447*, 510−518.
2. Turk, E., and Wright, E. M. (1997) Membrane topology motifs in the SGLT cotransporter family, *J. Membr. Biol. 159*, 1−20.
3. Eskandari, S., Wright, E. M., Kreman, M., Starace, D. M., and Zampighi, G. A. (1998) Structural analysis of cloned plasma membrane proteins by freeze-fracture electron microscopy, *Proc. Natl. Acad. Sci. U.S.A. 95*, 11235−11240.
4. Turk, E., Kim, O., le Coutre, J., Whitelegge, J. P., Eskandari, S., Lam, J. T., Kreman, M., Zampighi, G., Faull, K. F., and Wright, E. M. (2000) Molecular characterization of *Vibrio parahaemolyticus* vSGLT: A model for sodium-coupled sugar cotransporters, *J. Biol. Chem. 275*, 25711−25716.
5. Turk, E., Kerner, C. J., Lostao, M. P., and Wright, E. M. (1996) Membrane topology of the human Na^+/glucose cotransporter SGLT1, *J. Biol. Chem. 271*, 1925−1934.
6. Lo, B., and Silverman, M. (1998) Cysteine scanning mutagenesis of the segment between putative transmembrane helices IV and V of the high affinity Na^+/glucose cotransporter SGLT1: Evidence that this region participates in the Na^+ and voltage dependence of the transporter, *J. Biol. Chem. 273*, 29341−29351.
7. Levy, O., Dai, G., Riedel, C., Ginter, C. S., Paul, E. M., Lebowitz, A. N., and Carrasco, N. (1997) Characterization of the thyroid Na^+/I^- symporter with an anti-COOH terminus antibody, *Proc. Natl. Acad. Sci. U.S.A. 94*, 5568−5573.
8. Levy, O., De la Vieja, A., Ginter, C. S., Riedel, C., Dai, G., and Carrasco, N. (1998) N-Linked glycosylation of the thyroid Na^+/I^- symporter (NIS). Implications for its secondary structure model, *J. Biol. Chem. 273*, 22657−22663.
9. Jung, H., Rübenhagen, R., Tebbe, S., Leifker, K., Tholema, N., Quick, M., and Schmid, R. (1998) Topology of the Na^+/proline transporter of *Escherichia coli*, *J. Biol. Chem. 273*, 26400−26407.
10. le Coutre, J., Turk, E., Kaback, H. R., and Wright, E. M. (2002) Ligand-induced differences in secondary structure of the *Vibrio parahaemolyticus* Na^+/galactose cotransporter, *Biochemistry 41*, 8082−8086.
11. Greenfield, N. J. (1996) Methods to estimate the conformation of proteins and polypeptides from circular dichroism data, *Anal. Biochem. 235*, 1−10.
12. Sreerama, N., and Woody, R. W. (2000) Estimation of protein secondary structure from circular dichroism spectra: Comparison of CONTIN, SELCON, and CDSSTR methods with an expanded reference set, *Anal. Biochem. 287*, 252−260.
13. Sreerama, N., and Woody, R. W. (2004) On the analysis of membrane protein circular dichroism spectra, *Protein Sci. 13*, 100−112.
14. Wallace, B. A., Lees, J. G., Orry, A. J., Lobley, A., and Janes, R. W. (2003) Analyses of circular dichroism spectra of membrane proteins, *Protein Sci. 12*, 875−884.
15. Veenstra, M., Lanza, S., Hirayama, B. A., Turk, E., and Wright, E. M. (2004) Local conformational changes in the *Vibrio* Na^+/galactose cotransporter, *Biochemistry 43*, 3620−3627.
16. Xie, Z. Y., Turk, E., and Wright, E. M. (2000) Characterization of the *Vibrio parahaemolyticus* Na^+/glucose cotransporter: A bacterial member of the sodium/glucose transporter (SGLT) family, *J. Biol. Chem. 275*, 25959−25964.
17. Crameri, A., Whitehorn, E. A., Tate, E., and Stemmer, W. P. (1996) Improved green fluorescent protein by molecular evolution using DNA shuffling, *Nat. Biotechnol. 14*, 315−319.
18. Waddell, W. J. (1956) A simple ultraviolet spectrophotometric method for the determination of protein, *J. Lab. Clin. Med. 48*, 311−314.
19. Mao, D., Wachter, E., and Wallace, B. A. (1982) Folding of the mitochondrial proton adenosinetriphosphatase proteolipid channel in phospholipid vesicles, *Biochemistry 21*, 4960−4968.
20. Sreerama, N., Venyaminov, S. Y., and Woody, R. W. (1999) Estimation of the number of α-helical and β-strand segments in proteins using circular dichroism spectroscopy, *Protein Sci. 8*, 370−380.
21. Lau, S. Y., Taneja, A. K., and Hodges, R. S. (1984) Synthesis of a model protein of defined secondary and quaternary structure. Effect of chain length on the stabilization and formation of two-stranded α-helical coiled-coils, *J. Biol. Chem. 259*, 13253−13261.
22. Greenfield, N. J., and Hitchcock-DeGregori, S. E. (1993) Conformational intermediates in the folding of a coiled-coil model peptide of the N-terminus of tropomyosin and α,α-tropomyosin, *Protein Sci. 2*, 1263−1273.
23. Brahms, S., and Brahms, J. (1980) Determination of protein secondary structure in solution by vacuum ultraviolet circular dichroism, *J. Mol. Biol. 138*, 149−178.
24. Strickland, E. H. (1974) Aromatic contributions to circular dichroism spectra of proteins, *CRC Crit. Rev. Biochem. 2*, 113−175.
25. Martin, S. R., and Bayley, P. M. (1986) The effects of Ca^{2+} and Cd^{2+} on the secondary and tertiary structure of bovine testis calmodulin. A circular-dichroism study, *Biochem. J. 238*, 485−490.
26. Jacobs, R. E., and White, S. H. (1989) The nature of the hydrophobic binding of small peptides at the bilayer interface: Implications for the insertion of transbilayer helices, *Biochemistry 28*, 3421−3437.
27. Kabsch, W., and Sander, C. (1983) Dictionary of protein secondary structure: Pattern recognition of hydrogen-bonded and geometrical features, *Biopolymers 22*, 2577−2637.
28. Schwede, T., Kopp, J., Guex, N., and Peitsch, M. C. (2003) SWISS-MODEL: An automated protein homology-modeling server, *Nucleic Acids Res. 31*, 3381−3385.
29. Bustamante, C., and Maestre, M. F. (1988) Statistical effects in the absorption and optical activity of particulate suspensions, *Proc. Natl. Acad. Sci. U.S.A. 85*, 8482−8486.
30. Wallace, B. A., and Mao, D. (1984) Circular dichroism analyses of membrane proteins: An examination of differential light scattering and absorption flattening effects in large membrane vesicles and membrane sheets, *Anal. Biochem. 142*, 317−328.
31. Reizer, J., Reizer, A., and Saier, M. H. J. (1994) A functional superfamily of sodium/solute symporters, *Biochim. Biophys. Acta 1197*, 133−166.
32. Abramson, J., Smirnova, I., Kasho, V., Verner, G., Kaback, H. R., and Iwata, S. (2003) Structure and mechanism of the lactose permease of *Escherichia coli*, *Science 301*, 610−615.

33. Huang, Y., Lemieux, M. J., Song, J., Auer, M., and Wang, D. N. (2003) Structure and mechanism of the glycerol-3-phosphate transporter from *Escherichia coli*, *Science 301*, 616−620.
34. Hooft, R. W., Sander, C., Scharf, M., and Vriend, G. (1996) The PDBFINDER database: A summary of PDB, DSSP and HSSP information with added value, *Comput. Appl. Biosci. 12*, 525−529.
35. Visser, N. V., Hink, M. A., Borst, J. W., van der Krogt, G. N., and Visser, A. J. (2002) Circular dichroism spectroscopy of fluorescent proteins, *FEBS Lett. 521*, 31−35.
36. Veenstra, M., Turk, E., and Wright, E. M. (2002) A Ligand-dependent Conformational Change of the Na^+/Galactose Cotransporter of *Vibrio parahaemolyticus*, Monitored by Tryptophan Fluorescence, *J. Membr. Biol. 185*, 249−255.
37. Taroni, C., Jones, S., and Thornton, J. M., II (2000) Analysis and prediction of carbohydrate binding sites, *Protein Eng. 13*, 89−98.
38. Cabiaux, V., Oberg, K. A., Pancoska, P., Walz, T., Agre, P., and Engel, A. (1997) Secondary structures comparison of aquaporin-1 and bacteriorhodopsin: A Fourier transform infrared spectroscopy study of two-dimensional membrane crystals, *Biophys. J. 73*, 406−417.
39. Oberg, K. A., Ruysschaert, J. M., and Goormaghtigh, E. (2004) The optimization of protein secondary structure determination with infrared and circular dichroism spectra, *Eur. J. Biochem. 271*, 2937−2948.
40. Haris, P. I., Chapman, D., and Benga, G. (1995) A Fourier-transform infrared spectroscopic investigation of the hydrogen−deuterium exchange and secondary structure of the 28-kDa channel-forming integral membrane protein (CHIP28), *Eur. J. Biochem. 233*, 659−664.
41. Van Hoek, A. N., Wiener, M., Bicknese, S., Miercke, L., Biwersi, J., and Verkman, A. S. (1993) Secondary structure analysis of purified functional CHIP28 water channels by CD and FTIR spectroscopy, *Biochemistry 32*, 11847−11856.
42. Oberg, K. A., and Fink, A. L. (1998) A new attenuated total reflectance Fourier transform infrared spectroscopy method for the study of proteins in solution, *Anal. Biochem. 256*, 92−106.
43. Foster, D. L., Boublik, M., and Kaback, H. R. (1983) Structure of the lac carrier protein of *Escherichia coli*, *J. Biol. Chem. 258*, 31−34.
44. le Coutre, J., Narasimhan, L. R., Patel, C. K. N., and Kaback, H. R. (1997) The lipid bilayer determines helical tilt angle and function in lactose permease of *Escherichia coli*, *Proc. Natl. Acad. Sci. U.S.A. 94*, 10167−10171.
45. Berger, C., Weber-Bornhauser, S., Eggenberger, J., Hanes, J., Pluckthun, A., and Bosshard, H. R. (1999) Antigen recognition by conformational selection, *FEBS Lett. 450*, 149−153.
46. Bosshard, H. R. (2001) Molecular recognition by induced fit: How fit is the concept? *News Physiol. Sci. 16*, 171−173.
47. Provencher, S. W., and Glockner, J. (1981) Estimation of globular protein secondary structure from circular dichroism, *Biochemistry 20*, 33−37.

BI052160Z